SUPPLEMENTARY INFORMATION

This file includes:
Supplementary Text
Figs. S1 to S5
Tables S1 to S3
Captions for movies S1, S2, and S3
Other supplementary materials for this manuscript include the following:
Movies S1, S2, and S3

Supplementary Text

1. Node Design

Our proposed modular chain design currently aims to allow reconfigurability of fabricated structures. The contact area between the two nodes is important to the stability of the lattice structure, as it relates to the structural stability of the fabricated structures and constrains the options for providing effective coupling forces for the node design at different scales. Therefore, it is of our interest to understand how the geometry and size of the node design can affect the contact area between nodes.

As shown in Fig. 2D, the two opening angles at the base of the rhombic pyramid are:

$$\alpha = sin^{-1}\left(\frac{\sqrt{6}}{3}\right) \tag{1}$$

$$\beta = sin^{-1}\left(\frac{\sqrt{3}}{3}\right) \tag{2}$$

with the height

$$h = \frac{\sqrt{6}a}{3} \tag{3}$$

We can calculate the edge lengths of the rhombic pyramid as follows

$$b = \sqrt{(a * sin\beta)^2 + h^2} = a \tag{4}$$

$$c = \sqrt{(a * sin\alpha)^2 + h^2} = \frac{2\sqrt{3}a}{3} \tag{5}$$

Based on Heron's formula, the area of the shaded triangle (ΔABC) can be calculated based on the lengths of its sides by using the following equation:

$$A_{triangle} = \sqrt{s(s-a)(s-b)(s-c)} = \frac{\sqrt{2}a^2}{3} \tag{6}$$

where $s = \frac{a+b+c}{2}$ is defined as the semi-perimeter of the shaded triangle.

Therefore, the areas for coupling contact A and volume V of the rhombic pyramid are:

$$A = 4 \cdot A_{triangle} = \frac{4\sqrt{2}a^2}{3} \tag{7}$$

$$V = \frac{4\sqrt{3}a^3}{27} \tag{8}$$

These two parameters are important design factors that affect the selection of the coupling mechanism and the relative density of the assembled lattice structure.

2. Relative Density

The core of a densely assembled lattice structure is composed of closely packed octet-truss unit cells (Fig. S1). The relative density of the octet-truss structure, which is denoted by $\bar{\rho}$, is the ratio of the density of the lattice structure (the unit cell) to the density of the solid materials used to build the lattice (the struts). It can be calculated by using the following equation:

$$\bar{\rho} = \frac{m/v_{cell}}{m/v_{strut}} = \frac{v_{strut}}{v_{cell}} \tag{9}$$

where m is the mass of the lattice structure, v_{cell} is the volume of the bounding box (marked by dashed lines in Fig. S1) of the unit cell, and v_{strut} is the sum of the volumes of struts enclosed in the bounding box. The values of v_{cell} and v_{strut} can be calculated with the following equations:

$$v_{cell} = \sqrt{2}(l + 2h)^3 \tag{10}$$

$$v_{strut} = 12v_{link} = 12 \cdot (2v_{node} + v_{rod}) \tag{11}$$

$$v_{rod} = \pi(r_1 - r_0)^2 l \tag{12}$$

$$v_{node} = \frac{4\sqrt{3}a^3}{27} + \pi(r_2 - r_1)^2 d \tag{13}$$

where r_0, r_1, and r_2 are the inner radius of the rod, outer radius of the rod, and outer radius of coupling flange, respectively. Additionally, l is the length of the rod and d is the height of the coupling flange as shown in Fig. 2A. The values of these design parameters are listed in Table S1. Substituting these values and Eqs. (10) - (13) into Eq. (9), the relative density becomes

$$\bar{\rho} = \frac{12\cdot(2v_{node}+v_{rod})}{\sqrt{2}(l+2h)^3} = \frac{6\sqrt{2}(\frac{8\sqrt{3}a^3}{27}+2\pi(r_2-r_1)^2 d + \pi(r_1-r_0)^2 l)}{(l+2h)^3} \approx 1.66\% \tag{14}$$

Without considering the shape and volume of the node ($a = 0, d = 0, h = 0, r_2 = 0$), and only using solid struts ($r_0 = 0$), the relative density takes the form $\bar{\rho} = 6\sqrt{2}\pi(r_1/l)^2$, which has been used for idealized lattice structures (62). This equation slightly overestimates the relative density, however, because of the double-counting of the volume overlap at the nodes.

By varying the sizes of the rod and node, our modular chain design can potentially create various lattice structures with a large range of relative densities. For example, if the lengths of the rods and coupling flanges are all reduced to zero, the resulting lattice structure will be composed of densely packed stellated rhombic dodecahedrons with 100% relative density (Fig. 4F).

3. Stiffness and Strength Predictions of an octet-truss unit cell

Relative density is an important material parameter in the elastic compliance matrix. As shown in Fig. S1, the cubic symmetry property of the octet-truss lattice suggests the following linear elastic strain (ε_{ij}) and stress (σ_{ij}) tensor relationship (62) for pin-jointed struts (indices i, j are defined based on the coordinate system described in Fig. S1):

$$\begin{pmatrix} \varepsilon_{xx} \\ \varepsilon_{yy} \\ \varepsilon_{zz} \\ \varepsilon_{yz} \\ \varepsilon_{xz} \\ \varepsilon_{xy} \end{pmatrix} = \frac{1}{\bar{\rho}E_s} \begin{pmatrix} 9 & -3 & -3 & 0 & 0 & 0 \\ -3 & 9 & -3 & 0 & 0 & 0 \\ -3 & -3 & 9 & 0 & 0 & 0 \\ 0 & 0 & 0 & 12 & 0 & 0 \\ 0 & 0 & 0 & 0 & 12 & 0 \\ 0 & 0 & 0 & 0 & 0 & 12 \end{pmatrix} \begin{pmatrix} \sigma_{xx} \\ \sigma_{yy} \\ \sigma_{zz} \\ \sigma_{yz} \\ \sigma_{xz} \\ \sigma_{xy} \end{pmatrix} \tag{15}$$

where E_s is the Young's modulus of the strut material (2.25 GPa for ABS materials).

Based on our current folding algorithms, our 3D lattice structures are designed to support external loads mainly from their top and bottom (although the FCC crystalline structure is known to be relatively isotropic (61, 62, 64), therefore the mechanical properties of the assembled lattice structures along the Z direction is of the greatest interest. From Eq. (15), the following two stiffness predictions can be derived (64):

For the compressive modulus: $$E_{zz} = \frac{1}{9}\bar{\rho}E_s \approx 4.15\ MPa \tag{16}$$

For the shear modulus: $$G_{zx} = \frac{1}{12}\bar{\rho}E_s \approx 3.11\ MPa \tag{17}$$

As the relative density is only affected by the shape and size of the link design, the two moduli of the same lattice structure can be further increased if stronger materials are used to replace the ABS tubes.

Based on the geometries of the node and unit cell as shown in Fig. 2D and Fig. S1, we can further derive the following relationships between the coupling forces and external forces for the unit cell under different loading conditions:

Under compression forces:

$$F_{compression} = 4(F_{strut}^{axial} \sin 45^{\circ} + F_{strut}^{radial} \cos 45^{\circ}) \tag{18}$$

Under shear forces:

$$F_{shear} = 2\sqrt{2}(F_{strut}^{axial} \cos 45^{\circ} + F_{strut}^{radial} \sin 45^{\circ}) \tag{19}$$

where F_{strut}^{axial} and F_{strut}^{radial} are the sum of coupling forces acting along the axial and radial directions of each link at the node joint, respectively. Once assembled, the string connection between neighboring links is similar to a pin-joint. Therefore, the contribution to the stiffness due to the bending of the struts is negligible (64). And Eq. (18) and (19) become the followings under the pin-joint assumption:

$$F_{compression} = 4F_{strut}^{axial} \sin 45^{\circ} \tag{20}$$

$$F_{shear} = 2\sqrt{2}F_{strut}^{axial} \cos 45^{\circ} \tag{21}$$

where $$F_{strut}^{axial} = 4F_{coupling} \sin 30^{\circ} \tag{22}$$

The coupling forces, $F_{coupling}$ originate from the four faces of the rhombic pyramid node. In our current design, they equal to the magnetic forces from the two pairs of neodymium magnets (5N). Therefore, the current unit cell can approximately support either 28.3N compression or 20N shear forces. As we mentioned previously, our current prototype is a proof-of-concept design, therefore, both the stiffness predictions (the compressive and shear moduli) and the predicted compression and shear forces will increase once we choose a stronger strut material and incorporate stronger coupling methods into the node design (Table S2 and S3).

Supplementary Figures

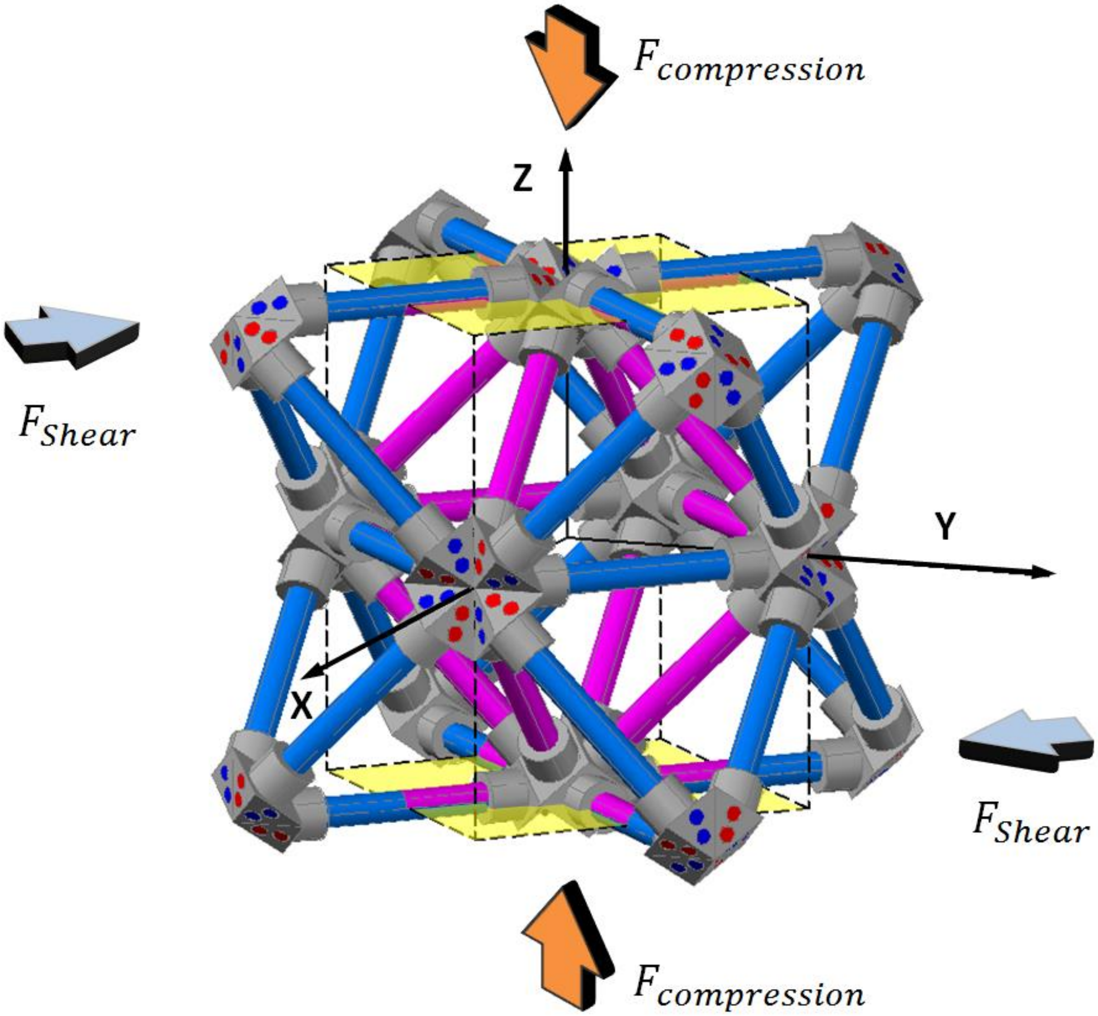

Fig. S1. 3D model of the unit cell inside a densely assembled octet-truss structure. The twelve struts counted in the calculation of the relation density ($\bar{\rho}$) of the octet-truss are enclosed inside the dashed rectangular box. The arrows illustrate the loading orientations of the compressive and shear forces that act on the shaded top and bottom planes.

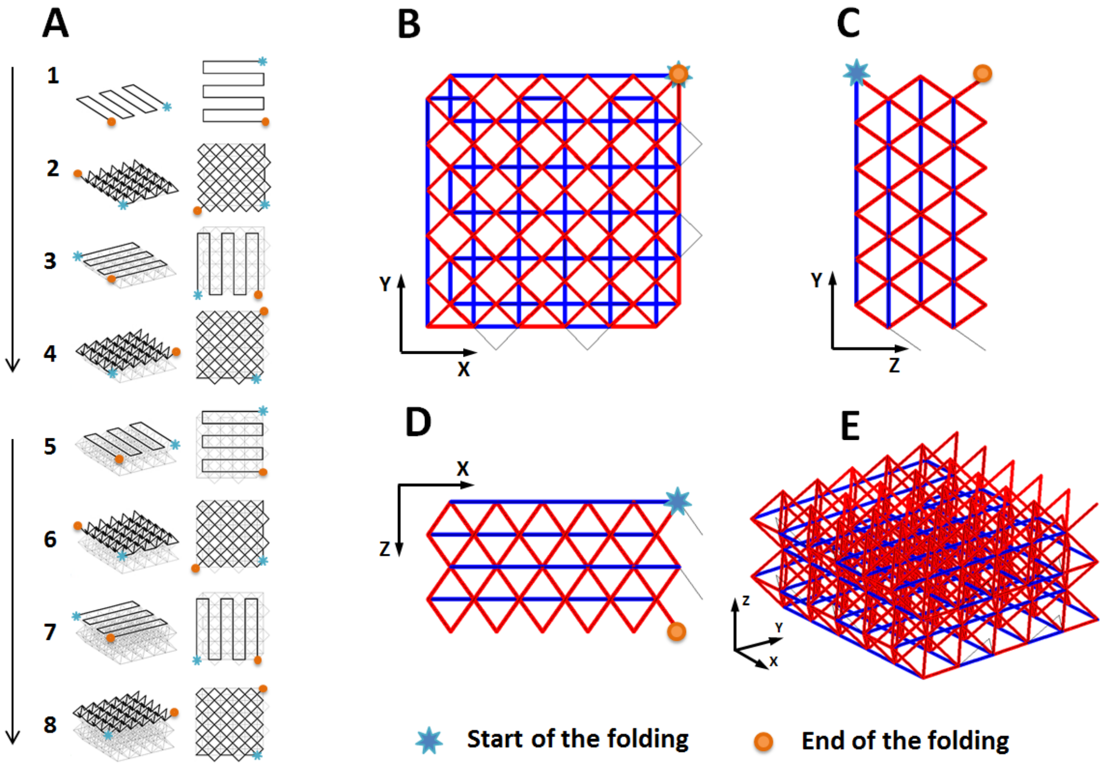

Fig. S2. Sparse folding algorithm for a rectangular lattice structure. (**A**) Schematic showing four different folding layers for the lattice structure. Odd and even numbers of layers use stripe and zigzag patterns, respectively. (**B** to **D**) Top, left, and back views of the rectangular lattice structure. The end of folding step 4 coincides with the start of step 1 on the X-Y plane. Also, steps 1-4 are idential to steps 5-8 on the X-Y plane. (**E**) 3D view of the rectangular lattice structure (5x5x2) that can be assembled from a 652-link chain. *Note:* Colored lattice is the core that has nodal connetivity of ten.

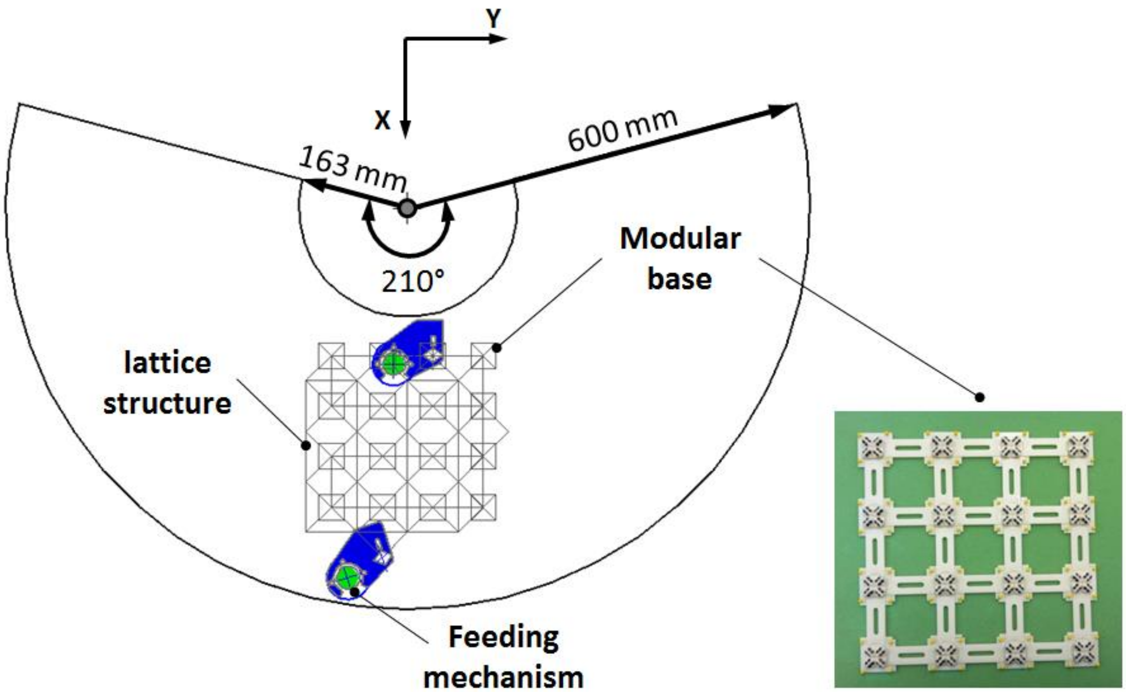

Fig. S3. The workspace of the robotic platform on X-Y plane. Shaded areas represents the projection of the feeding mechanism at extreme positions on the X-Y plane during the robotic assembly process. Due to the limitation of the workspace, a 3x3x2 sparse lattice structure (287-link) was robotically assembled to demonstrate our design efficacy. *Note:* Modular bases composed of 4-node joint connections are used for anchoring the first layer of the 3D lattice structure.

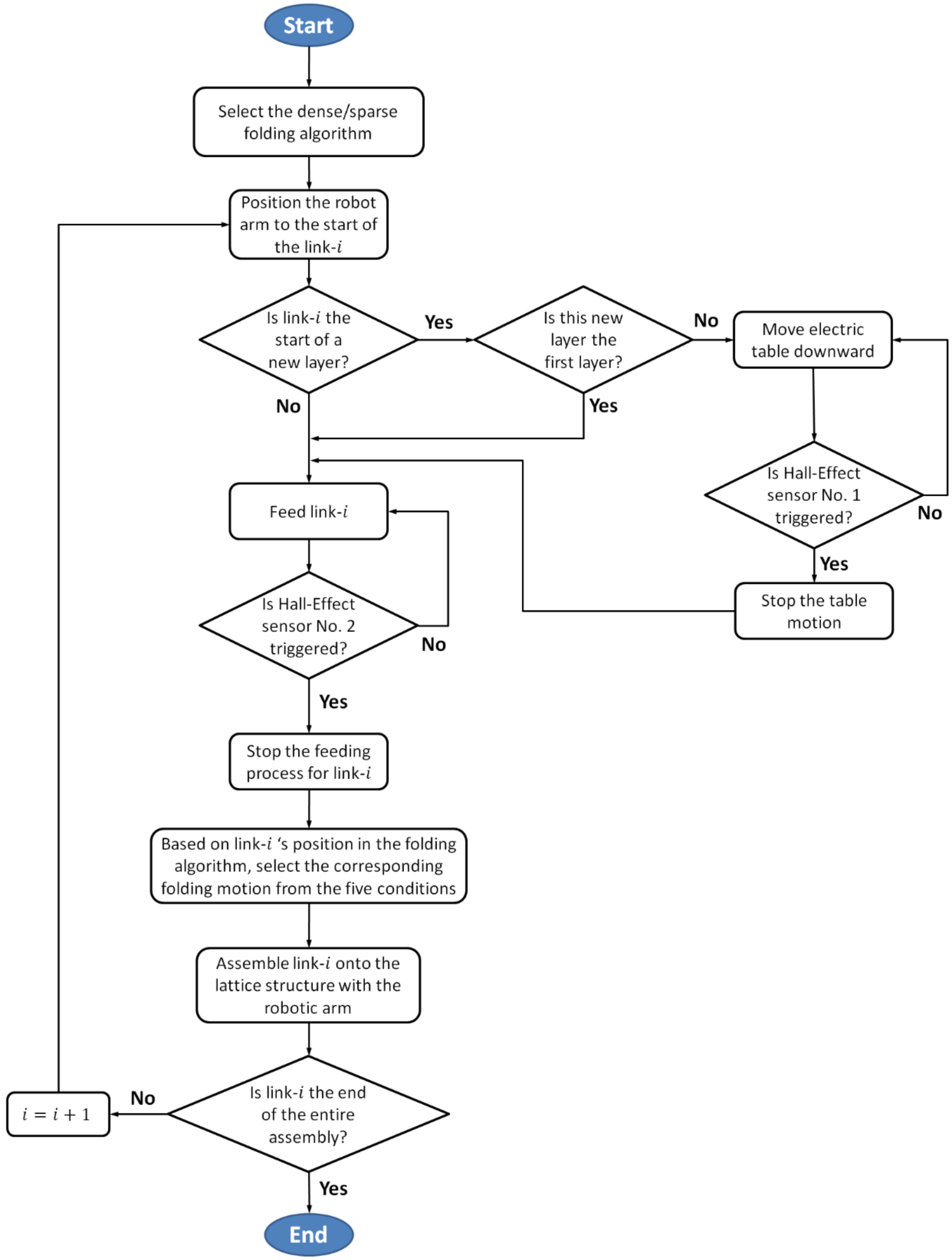

Fig. S4. The robotic assmbly process of the ith link of a lattice structure.

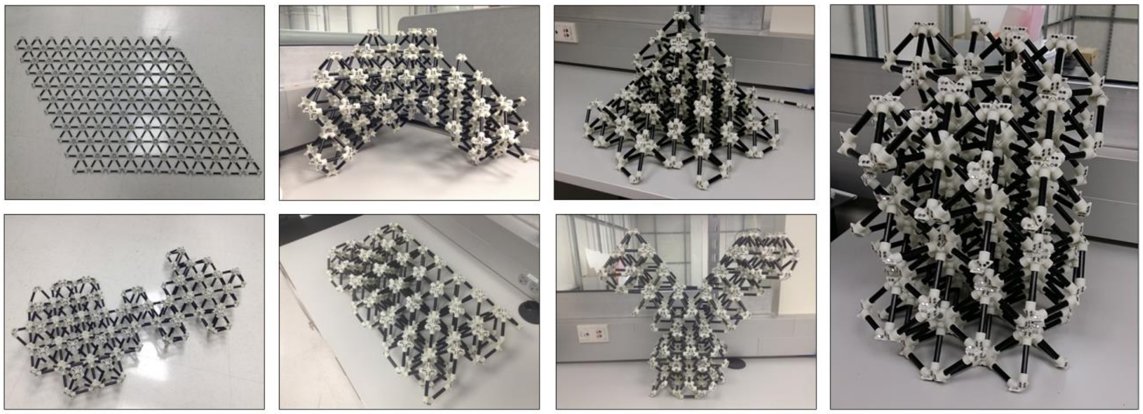

Fig. S5. Examples of the 2D and 3D structures that can be built by using alternative folding algorithms. *Note:* Except for the 2D structure, other 3D structures require robotic platform and folding algorithm that are different from our current method.

Supplementary Tables

Table S1. Design parameters and values for the link of modular chain.

Parameter	Description	Value	Unit
a	Edge length of the base of the rhombic pyramid	14.1	mm
b	Edge length of the shaded triangle	14.1	mm
c	Edge length of the shaded triangle	16.3	mm
d	Height of the coupling flange	8.0	mm
h	Height of the rhombic pyramid (node)*	11.5	mm
l	Length of the rod	53.0	mm
r_0	Inner radius of the rod	1.6	mm
r_1	Outer radius of the rod	3.2	mm
r_2	Outer radius of the coupling flange	5.5	mm
s	Semi-perimeter of the shaded triangle	22.3	mm
α	Opening angle at the base of the rhombic pyramid	54.74	degree
β	Opening angle at the base of the rhombic pyramid	35.26	degree
$A_{triangle}$	Area of the shaded triangle	93.7	mm^2
A	Area of the rhombic pyramid for coupling contact	374.9	mm^2
V	Volume of the rhombic pyramid (node)	719.3	mm^3

* Before 3D-printing, the tip of the rhombic pyramid (node) in the CAD is chopped off (3 mm height) to allow space for the double-knot. Therefore, the length of each link is calculated as $2(h-3)+l$ = 70mm.

Table S2. Variables and values used in predictions of mechanical properties for the octet-truss unit cell.

Parameter	Description	Value	Unit
$\bar{\rho}$	Relative density of the octet-truss	1.66%	-
v_{cell}	Volume of the unit cell	~5.60x10^{-4}	m^3
v_{strut}	Sum of the volumes of the struts within a unit cell	~9.27x10^{-6}	m^3
ε	Elastic strain	-	-
σ	Stress	-	Pa
E_s	Young's modulus of the strut material (ABS)	2.25 x10^9	Pa
E_{zz}	Compressive modulus of the truss	4.15x10^6	Pa
G_{zx}	Shear modulus of the truss	3.11x10^6	Pa
$F_{compression}$	Compressive force supported by unit cell	28.3	N
F_{shear}	Shear force supported by the unit cell	20.0	N
$F_{coupling}$	Total coupling forces at the nodes	5	N
F_{strut}^{axial}	Sum of the coupling forces in the axial direction	10	N
F_{strut}^{radial}	Sum of the coupling forces in the radial direction	-	N

Table S3. Parameters used in predictions of the unit cell's compression and shear forces based on existing designs of different coupling mechanisms.

Citation	**Coupling mechanism**	**Actuation method**	**Reported $F_{coupling}$ (N)**	**Contact areas (mm^2)**	**Compatible node size* a (mm)**	**Predicted $F_{compression}/F_{shear}$ (N)**
(9)	Permanent magnets	SMA	80	60x60	124	452.5/320.0
(8)	Mechanical hook	DC motor	200	~55x55	113	1131.4/800.0
(10)	Permanent magnets	DC motor	60	100x100	206	339.4/240.0
(70)	Mechanical locking bolts	DC motor	4000	105x105	216	22627.4/16000.0
(71)	Binder materials	Heat	173	55x55	113	978.6/692.0
(72)	Electro-permanent Magnets	Current pulse	88.4	42x42	87	500.1/353.6
This work	Permanent magnets	N/A	5.0	15.9	14.1	28.3/20.0

*Calculation of the compatible node size is based on the largest square (the contact area) which can be inscribed in the shaded triangle ΔABC (Fig. 2D): $a = \frac{(3+2\sqrt{2})x}{2\sqrt{2}}$, where x the length of the square from the reported contact areas.

Supplementary Movies

Movie S1:

The process of disassembling and recycling the reconfigurable modular chain. After each robotic assembly process, the lattice structure is designed to be manually disassembled. For a 287-link chain, this manual disassembly process can be finished within 70 seconds.

Movie S2:

Robotic assembly of a small 2D lattice structure. 3-node modular bases are required during assembly. Compared to the 3D assembly process, the complexity involved in the 2D assembly is much easier. Therefore, a small 2D structure (14-link) is used to validate the design efficacy.

Movie S3:

Robotic assembly of a 3x3x2 3D lattice structure (304(L) x 304(W) x 215(H) mm) with 287 links. 4-node modular bases are required for the first layer. Compared to the folding process used for assembling 3D dense lattice structure, the assembly of a sparse lattice structure is more challenging since it involves forming lower nodal connectivity of ten.